Annihilation dynamics of umbilical defects in nematic liquid crystals under applied electric fields

I. Dierking,* O. Marshall, J. Wright, and N. Bulleid
School of Physics and Astronomy, University of Manchester, Schuster Building, Oxford Road, Manchester M13 9PL, United Kingdom
(Received 24 February 2005; published 28 June 2005)

Umbilical defects were induced in a nematic liquid crystal with negative dielectric anisotropy, confined to Hele-Shaw cells with homeotropic boundary conditions, and their annihilation dynamics were investigated experimentally. Dynamic scaling laws, previously proposed for Schlieren defects, were verified also for electric field induced umbilical defects while varying external parameters, such as electric field amplitude, frequency, Hele-Shaw cell gap, and temperature. In all cases, scaling relations of $\rho(t) \propto t^{-1}$ for the defect density and $D \propto (t_0 - t)^{1/2}$ for the defect pair separation were obtained, independent of external field parameters. The experimental results give evidence of the universality of scaling relations for the annihilation of topological defects in liquid crystals, extended to umbilical defects and their annihilation dynamics under applied external fields.

DOI: 10.1103/PhysRevE.71.061709 PACS number(s): 61.30.Jf, 61.72.Cc

I. INTRODUCTION

Coarsening phenomena in general have been a long-standing topic in condensed matter physics on both the experimental and the theoretical levels [1,2]. This is due to the fundamental effects that coarsening exhibits on the physical properties of materials and thus their applicability in devices. Materials studied cover the whole range of condensed matter, from the well known metal alloys all the way to liquid crystals, or even biologically engineered systems. Due to their extremely small elastic constants and their intrinsic birefringence, liquid crystals are ideal materials for the study of coarsening processes, because the motion of defects can be followed *in situ* through polarizing optical microscopy on practical spatial and temporal scales.

Liquid crystals (LCs) [3,4] are anisotropic fluids, thermodynamically located between the isotropic liquid and the three-dimensionally ordered crystal. Various mesogenic phases are observed, often identified by their characteristic textures [5], which exhibit a wealth of different topological defects. The simplest of the liquid crystal phases is the nematic, which exhibits solely orientational order of the long axes of rod shaped molecules, while the molecular centers of mass are isotropically distributed. The nematic phase is the least ordered of the LC phases, the one with the highest symmetry. It is generally observed as the first low temperature phase to the isotropic liquid. A common polarizing microscopic texture of the nematic phase is that of the *Schlieren texture*, which exhibits brushes that converge at singular points under planar boundary conditions [5]. These singularities are topological defects of different strength and sign, twofold brushes of strength $s = \pm 1/2$ and fourfold brushes of strength $s = \pm 1$ [6,7] [Figs. 1(a) and 2(a)]. The sign of the defect strength can be determined by rotation of the crossed polarizers. Generally, all four different defects occur within a sample, but there are no isolated point defects observed; all defects are all connected, as evidenced via the brushes. The sum over all defect strengths of a large sample tends to vanish. The macroscopic defect distribution is not static, but defects of equal strength and opposite sign attract each other and eventually annihilate with time, ideally resulting in a uniformly oriented liquid crystal director distribution.

When a nematic material with negative dielectric anisotropy ($\Delta\varepsilon < 0$) is subjected to homeotropic boundary conditions (director perpendicular to the bounding glass plates), application of an electric field along the director will cause a reorientation into the planar configuration once the Fréeder-

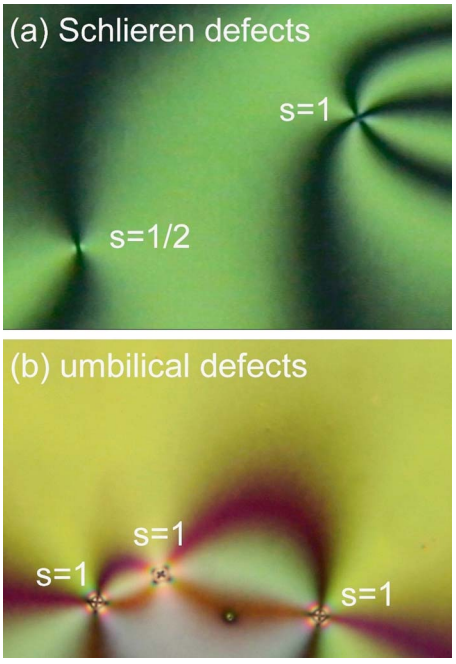

FIG. 1. (Color online) Texture examples of (a) Schlieren defects obtained through thermally quenching across the isotropic-nematic phase transition and (b) umbilical defects induced by electric field application to a nematic liquid crystal with negative dielectric anisotropy under homeotropic boundary conditions. In the case of nematic Schlieren textures four different defects may be observed: $s = \pm 1/2$ and ± 1, while umbilical defects are only of strength $s = \pm 1$.

*Author to whom correspondence should be addressed. Electronic address: ingo.dierking@manchester.ac.uk

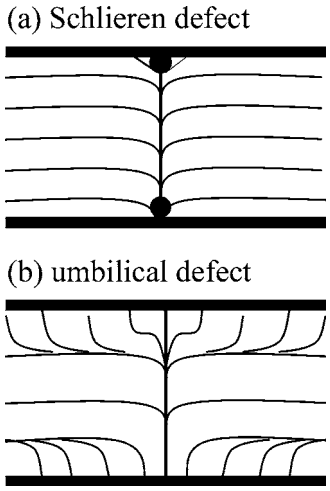

FIG. 2. Schematic director field representation of (a) an $s=\pm 1$ Schlieren defect ending in singular points and (b) an $s=\pm 1$ electric field induced umbilical defect without singularities. The figure represents a vertical cut through the defect core (after [9]).

icksz threshold is exceeded. Under these conditions only two types of director field deformations can be formed, which are very similar to the s=±1 Schlieren point defects, but differ in so far as the director continuously tilts toward the substrate normal, being parallel to it at the core of the defect [[4], Chap. 3.5]. Such defects are called *umbilical defects* [8] [Figs. 1(b) and 2(b)] and do not end in singular points [9]. Note also the difference of the optical texture between Schlieren and umbilical defects very close to the defect core (Fig. 1). Umbilical defects have experimentally been observed before [9,10] and their annihilation dynamics is the subject of this paper.

The coarsening dynamics of liquid crystal defects has been studied on several occasions with respect to scaling laws, both experimentally [11–18] and theoretically or through computer simulations in two- as well as three-dimensional systems [19–23]. Much of the reported experimental work is related to the annihilation of string defects [11–14] and defect loops [14,18], while the annihilation of point defects is discussed in Refs. [15–17]. It is worthwhile to point out that there have also been experimental investigations reported for the $s=\pm 1$ point defect annihilation in smectic-*C* materials [24] as well as nematic polymers [25,26], which led to similar scaling results as observed for the low molecular nematic systems.

From experimental investigations the following scaling laws for liquid crystal topological defect annihilation seem to be obeyed, although slight deviations have been suggested by computer simulation work [20–23]: (i) point defect density or string density $\rho(t)$:

$$\rho(t) \propto t^{-\nu} \tag{1}$$

with $\nu=1$; (ii) point defect separation or loop diameter $D(t)$:

$$D(t) \propto (t_0 - t)^{\alpha} \tag{2}$$

with t_0-t the time to annihilation and $\alpha=1/2$.

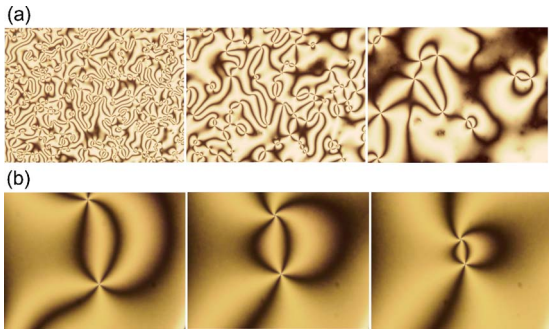

FIG. 3. (Color online) Exemplary time series of umbilical defect annihilation under applied electric fields: (a) $t=5$ (left), 30 (middle), and 80 s (right) at cell gap $d=6$ μm, electric field amplitude $E=2$ V μm^{-1}, and frequency $f=300$ Hz, typical for the determination of the defect density scaling exponent ν; (b) $t_0-t=880$ (left), 410 (middle), and 80 s (right) for cell gap $d=50$ μm at $E=4$ V μm^{-1} and $f=300$ Hz, typical for the determination of the pair separation scaling exponent α. Similar texture images were observed throughout varying experimental conditions. Each image size is 1280 $\times$960 pixels, corresponding to 520$\times$390 μm^2.

Relations (1) and (2) were suggested from dimensional analysis of the equation of motion of defects, derived by accounting for the force between a defect and all other defects balanced by a dissipative force proportional to the velocity [16,17], i.e., viscous behavior in the mean-field limit. As pointed out in these references, the equation of motion is equivalent to that of vortices in the *XY* model [19]. It should be noted that relations (1) and (2) with $\nu=1$ and $\alpha=1/2$, respectively, are valid for two-dimensional systems only. Further, we note that in our investigation below, *D* refers to the distance between two annihilating defects, not the average distance between neighboring defects λ, which would be directly related to the defect density via $\lambda \sim \rho^{-1/2}$.

Generally, the formation of defects is induced by either pressure [13–15,18] or temperature [15,24–26] quenches across the isotropic to nematic phase transition; thus through a sudden change of the free energy of the system. This often leads to a variety of defects observed. Similarly, the application of an electric field changes the free energy. But for appropriate material selection and boundary conditions, this induces umbilical defects, defects of only the $s=\pm 1$ type. The annihilation dynamics of electric field induced umbilical defects has only been investigated very rarely [16,17], with no dependence on external field parameters reported. The present study investigates in detail the influence of electric field amplitude, field frequency, cell gap, and temperature on the dynamic scaling laws of nematic umbilical defect annihilation.

II. EXPERIMENT

The liquid crystal employed in this investigation was a commercially available mixture ZLI-2806 (Merck, Darmstadt), with a phase sequence on cooling given by Iso $\overset{100\ °C}{\leftrightarrow}$ N $\overset{-20\ °C}{\leftrightarrow}$ cryst, and is thus a liquid crystal with a very wide nematic phase range and exhibiting the nematic phase

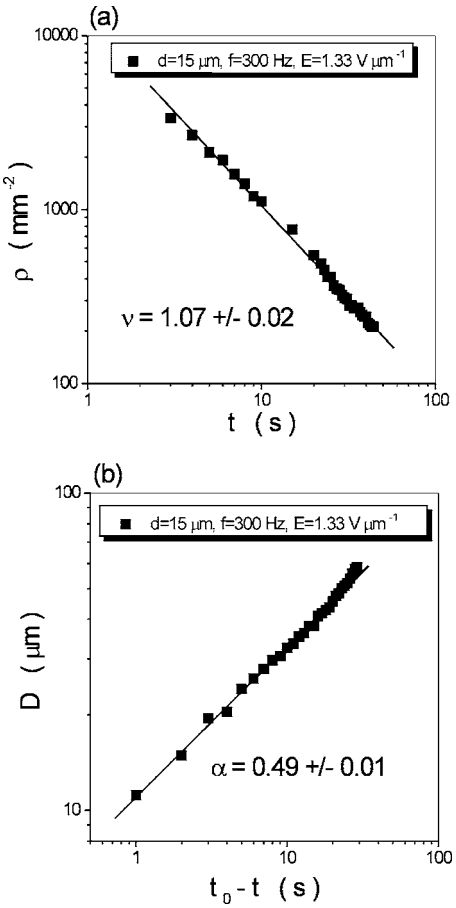

FIG. 4. Exemplary experimental data for the determination of (a) the defect density annihilation exponent ν and (b) the defect pair annihilation separation exponent α for umbilical defects induced at cell gap $d=15$ μm, electric field amplitude $E=1.33$ V μm^{-1}, and frequency $f=300$ Hz. Equivalent data were observed for varying external conditions.

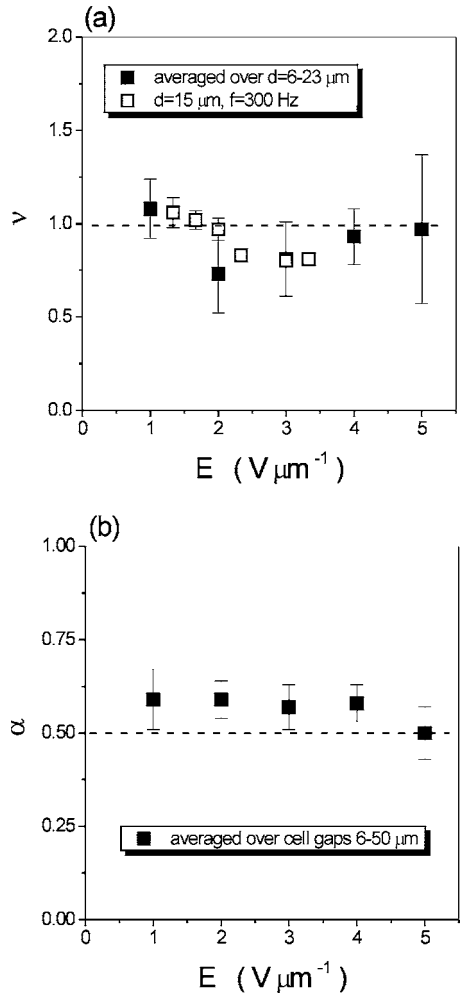

FIG. 5. Exponents for the annihilation dynamics of umbilical defects as a function of applied electric field E: (a) ν for the defect density, and (b) α for the defect pair separation.

at room temperature. The LC mixture has a negative dielectric anisotropy of $\Delta\varepsilon=-4.8$ at $T=20$ °C and $f=1$ kHz and was capillary filled into sandwich cells of gaps between 6 and 50 μm with homeotropic boundary conditions, obtained by substrate treatment with JALS 240-R40, a special polyimide (JSR Electronics, Leuven) promoting homeotropic alignment. Umbilical defects were induced by square wave electric field application through a function generator (TTi TG1010) in combination with an in house built high voltage amplifier. Electric fields were applied throughout the observation of the annihilation process and varied between $E=1$ and 5 V μm^{-1} for frequencies of $f=1$–10^6 Hz. Temperatures were controlled with a Linkham TMS91 hot stage and controller. Microscopic textures were recorded by polarizing microscopy (Nikon Optiphot-pol) in conjunction with digital image acquisition (JVC KY-F1030) at a maximum time resolution of 1 s and spatial resolution of 1280×960 pixels, corresponding to an image size of 520×390 μm^2. Subsequent image analysis with respect to the number density and separation of umbilical defects was carried out with software IMAGETOOL3.0, developed at the University of Texas Health Science Center, San Antonio.

III. RESULTS AND DISCUSSION

Figure 3 depicts a typical polarizing microscopic texture example of the observed experimental time development of umbilical defect annihilation as used for the determination of the scaling relations of (a) the defect density ρ(t), Eq. (1), and (b) the pair defect separation $D(t)$, Eq. (2). Application of an electric field to a homeotropically oriented sample of the liquid crystal with negative dielectric anisotropy results in the formation of numerous $s=\pm1$ umbilical defects, which mutually annihilate with proceeding time, thus reducing the number of observed defects [Fig. 3(a)]. Generally, not all of the defects vanish at long time scales, due to pinning at substrate irregularities and impurity inclusions, leaving a small number of remaining static defects. Individual defects of opposite sign attract each other and approach eventual annihilation with increasing velocity for decreasing spatial separation [Fig. 3(b)].

The respective scaling relations of Eqs. (1) and (2) are exemplary demonstrated in Fig. 4, with part (a) showing the temporal decrease of the defect density and (b) that of the pair defect separation, t_0-t indicating the time to annihila-

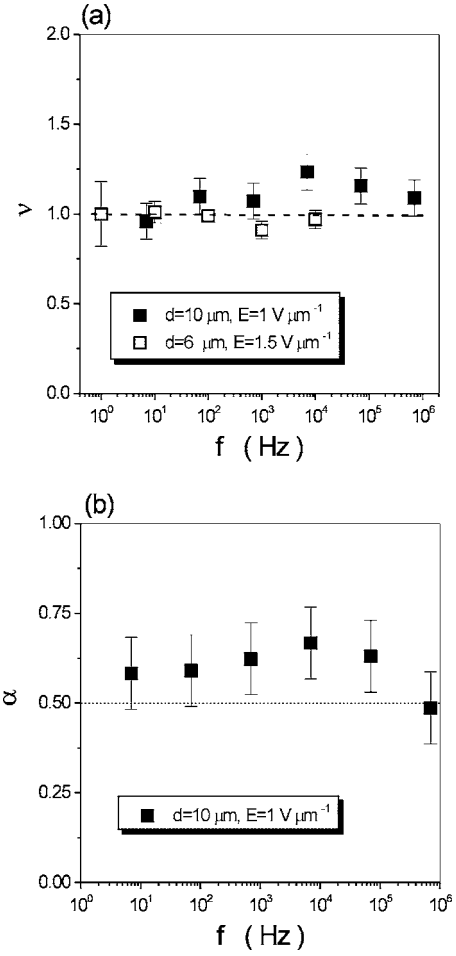

FIG. 6. Exponents for the annihilation dynamics of umbilical defects as a function of applied electric field frequency f: (a) ν for the defect density, and (b) α for the defect pair separation.

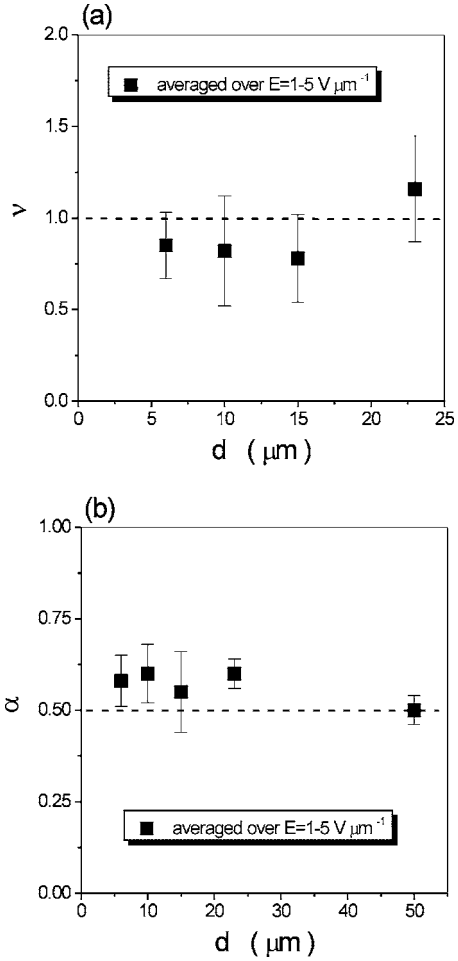

FIG. 7. Exponents for the annihilation dynamics of umbilical defects as a function of sandwich cell gap d: (a) ν for the defect density, and (b) α for the defect pair separation. For large cell gaps ($d \geqslant 50$ μm) the number of generated defects was too small for a reasonable analysis of the defect density decay exponent ν.

tion. Within the limits of experimental error, scaling exponents of $\nu=1$ and $\alpha=1/2$ are obtained, respectively. Scaling is typically observed over more than one order of magnitude and the scaling exponents for the umbilical defects are in agreement with those obtained for Schlieren defects generated by pressure or temperature quenches.

In the following, we examine the effects of external parameter variation on the scaling exponents ν and α for the defect density $\rho(t)$ and the pair separation $D(t)$, respectively. Figure 5 depicts the results for varying electric field amplitude E, averaged for various cell gaps between $d=6$ and 23 μm for the defect density [Fig. 5(a)] and $d=6$ and 50 μm for the pair separation [Fig. 5(b), shown by the closed symbols. For the $d=50$ μm cell only very few defects could be induced; thus a scaling analysis according to Eq. (1) was not appropriate. The open symbols of Fig. 5(a) represent the results of an independent control experiment performed with an additional cell. Error bars indicate the range of values obtained from several experiments. Within the limits of error, both scaling exponents are apparently independent of applied electric field amplitude and in general accordance with the expected values of $\nu=1$ and $\alpha=1/2$ for defect density and pair separation, respectively.

Figure 6 shows the dependence of the scaling exponents on the frequency of the applied electric field at an amplitude of $E=1$ V μm^{-1} (closed symbols). Again, the open symbols of Fig. 6(a) represent the results of an independent control experiment at slightly smaller cell gap and slightly higher field amplitude. Also with respect to applied electric field frequency the scaling exponents are practically constant with $\nu=1$ for the defect density and $\alpha=1/2$ for the defect pair separation.

The dependence of the two scaling exponents ν and α on sandwich cell gap d is depicted in Figs. 7(a) and 7(b) for the defect density and the defect pair separation, respectively. Also here the predicted behavior of $\nu=1$ and $\alpha=1/2$ is observed, with no apparent cell gap dependence to be detected in the ranges of d=6–23 μm for the defect density and d =6–50 μm for the defect pair separation. As mentioned above, the small number of defects induced for the d =50 μm cell makes an analysis with respect to the exponent ν inappropriate. Figure 8 demonstrates that the predicted scaling relations are also independent of temperature over a wide range of the existence of the nematic phase. Only close to the clearing temperature are deviations observed. A similar result as compared to Fig. 8(a) was obtained for the defect

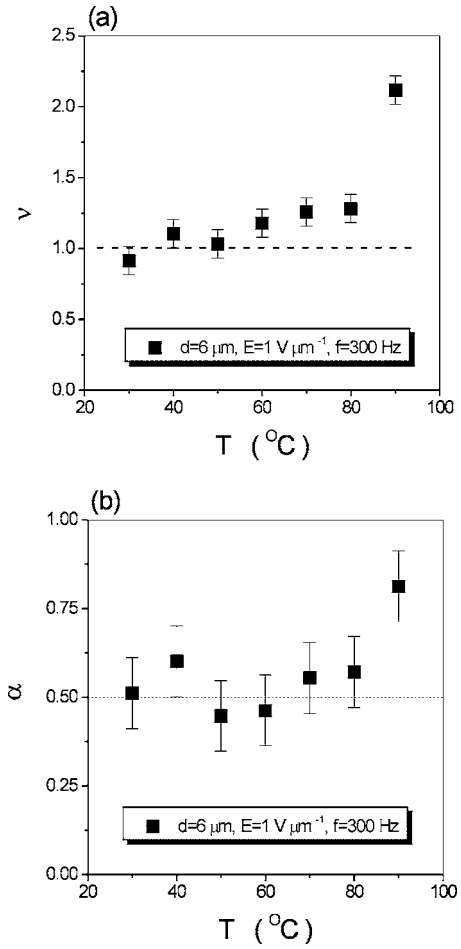

FIG. 8. Exponents for the annihilation dynamics of umbilical defects as a function of temperature T: (a) ν for the defect density, and (b) α for the defect pair separation. Deviations from the general behavior of $\nu=1$ and $\alpha=1/2$ are observed in the very close vicinity of the clearing point.

density by Monte Carlo simulations [23] and was attributed to a dominance of interparticle forces over Brownian forces at lower temperatures.

In all of our parameter variation series we obtain scaling exponents of approximately $\nu=1$ and $\alpha=1/2$, which is consistent with the rate-equation analysis given in [16,17]. As pointed out in [27], fluctuations would reduce the defect density exponent to $\nu<1$. Within the limits of experimental error we cannot draw any conclusions with respect to such behavior. On occasion we obtain exponents ν slightly larger than 1, but without any significant trends observed. We are thus hesitant to assign these values to a meaningful interpretation beyond that of the rate-equation analysis, $\nu=1$, although effects of deviation from a true two-dimensional situation may play a role.

Most of the results reported here for the pair separation exponent α were obtained under conditions when the pair separation D was larger than the confining cell gap d, i.e., $D>d$. It is thus worthwhile to examine a possible change of exponent as the regime $D>d$ crosses over to $D<d$. Corresponding measurements were carried out for the thick cell of $d=50$ μm and are depicted in Fig. 9. We did not observe any

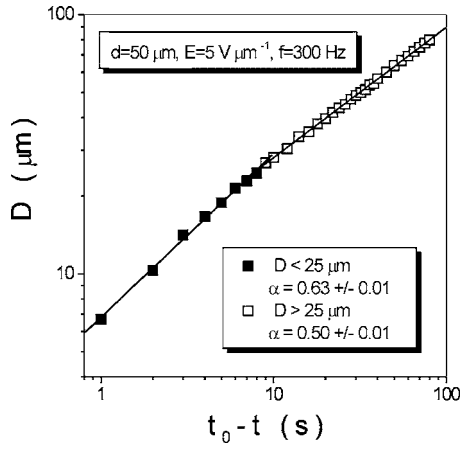

FIG. 9. Closeup data for the time evolution of the defect pair separation D for the thick cell of gap $d=50$ μm. No significant change of the dynamic scaling exponent α can be detected as the pair defect separation D crosses over from $D>d$ to $D<d$.

change in the scaling exponent α at $D=d=50$ μm, although it appears that α increases slightly from $\alpha=0.50\pm0.01$ to 0.63 ± 0.01 on decreasing defect pair separation below $D=d/2$. Nevertheless, it should be noted that this change is very close to the limit of experimental reproducibility, which is approximately given by $\Delta\alpha=\pm0.1$. In particular, we do not observe the change from $\alpha=1$ to $1/2$ on approaching annihilation, as has been reported for $s=\pm1$ defects created by thermal quenching of free-standing Sm-C films [24]. The annihilation dynamics of nematic umbilical defects rather appears to follow the general prediction of Eq. (2), independent of sample size.

In thick cells of $d=50$ μm we occasionally also observed the formation of defect loops, which were completely absent in samples of smaller substrate spacing. Determination of the dynamic scaling exponent of loop collapse (Fig. 10) yields values close to $\alpha=1/2$, which are consistent with previously reported data on low molar mass [14,18], as well as polymeric nematic liquid crystals [26], again within the limits of experimental reproducibility.

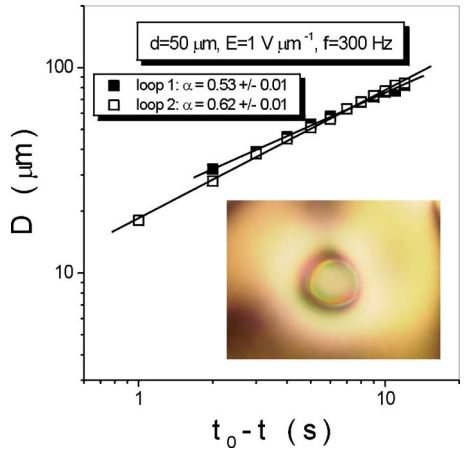

FIG. 10. (Color online) Annihilation dynamics of type-1/2 disclination line loops, occasionally observed in thick cells of gap $d=50$ μm. The loop diameter D collapses according to the predicted scaling law $D\propto(t_0-t)^{1/2}$, with t_0-t the time to annihilation.

IV. CONCLUSIONS

The annihilation dynamics of nematic umbilical defects, induced by electric field application to homeotropically oriented liquid crystal samples of negative dielectric anisotropy, was experimentally investigated with respect to scaling laws for the defect density $\rho(t) \propto t^{-\nu}$ and the defect pair separation $D \propto (t_0 - t)^{\alpha}$. Detailed studies were carried out varying the electric field amplitude, frequency, sample cell gap, and temperature. In all cases scaling exponents of $\nu = 1$ and $\alpha = 1/2$ were obtained for the defect density and the pair separation, respectively. The systematic investigations demonstrate that the annihilation dynamics of electric field induced umbilical defects is equivalent to that of $s = \pm 1$ Schlieren defects generated by thermal or pressure quenches across the isotropic to nematic liquid crystal phase transition, thus signifying the universality of the proposed scaling behavior. No significant deviations from the predicted scaling laws were observed at the crossover from three- to two-dimensional systems. Analysis of the occasional observation of type-1/2 defect loops at large sample dimensions verifies previously reported results.

ACKNOWLEDGMENTS

The authors would like to thank K. Tarumi of Merck, Darmstadt, for generously providing the liquid crystal mixture employed in this investigation. We are also thankful for the financial support of the Nuffield Foundation under Grant No. NAL/00680/G.

[1] L. Ratke and P. W. Voorhees, *Growth and Coarsening* (Springer, Berlin, 2002).
[2] A. J. Bray, Adv. Phys. **43**, 357 (1994).
[3] P. G. de Gennes and J. Prost, *The Physics of Liquid Crystals*, 2nd ed. (Clarendon Press, Oxford, 1993).
[4] S. Chandrasekhar, *Liquid Crystals*, 2nd ed. (Cambridge University Press, Cambridge, U.K., 1992).
[5] I. Dierking, *Textures of Liquid Crystals* (Wiley-VCH, Weinheim, 2003).
[6] M. Kléman, *Points, Lines and Walls* (Wiley, Chichester, 1983).
[7] H.-R. Trebin, Adv. Phys. **31**, 195 (1982).
[8] A. Rapini, J. Phys. (Paris) **34**, 629 (1973).
[9] A. Saupe, Mol. Cryst. Liq. Cryst. **21**, 211 (1973).
[10] R. B. Meyer, Mol. Cryst. Liq. Cryst. **16**, 355 (1972).
[11] H. Orihara and Y. Ishibashi, J. Phys. Soc. Jpn. **55**, 2151 (1986).
[12] H. Orihara and T. Nagaya, J. Phys. Soc. Jpn. **56**, 3086 (1987).
[13] I. Chuang, R. Durrer, N. Turok, and B. Yurke, Science **251**, 1336 (1991).
[14] I. Chuang, N. Turok, and B. Yurke, Phys. Rev. Lett. **66**, 2472 (1991).
[15] A. Pargellis, N. Turok, and B. Yurke, Phys. Rev. Lett. **67**, 1570 (1991).
[16] T. Nagaya, H. Hotta, H. Orihara, and Y. Ishibashi, J. Phys. Soc. Jpn. **60**, 1572 (1991).
[17] T. Nagaya, H. Hotta, H. Orihara, and Y. Ishibashi, J. Phys. Soc. Jpn. **61**, 3511 (1992).
[18] I. Chuang, B. Yurke, A. N. Pargellis, and N. Turok, Phys. Rev. E **47**, 3343 (1993).
[19] H. Toyoki, Phys. Rev. A **42**, 911 (1990).
[20] M. Mondello and N. Goldenfeld, Phys. Rev. A **42**, 5865 (1990).
[21] H. Toyoki, Phys. Rev. E **47**, 2558 (1993).
[22] W. G. Jang, V. V. Ginzburg, C. D. Muzny, and N. A. Clark, Phys. Rev. E **51**, 411 (1995).
[23] C. Liu and M. Muthukumar, J. Chem. Phys. **106**, 7822 (1997).
[24] A. N. Pargellis, P. Finn, J. W. Goodby, P. Panizza, B. Yurke, and P. E. Cladis, Phys. Rev. A **46**, 7765 (1992).
[25] D.-K. Ding and E. L. Thomas, Mol. Cryst. Liq. Cryst. Sci. Technol., Sect. A **241**, 103 (1994).
[26] W. Wang, T. Shiwaku, and T. Hashimoto, J. Chem. Phys. **108**, 1614 (1998).
[27] V. V. Ginzburg, L. Radzihovsky, and N. A. Clark, Phys. Rev. E **55** 395 (1997).